ADVANCED MATERIALS TECHNOLOGIES
www.advmattechnol.de

Determination of Binary Interaction Parameters for Ternary Polymer–Polymer–Solvent Systems Using Raman Spectroscopy

Víctor-Alfonso Gracia-Medrano-Bravo, Lisa Merklein,* Nikolas Oberle, Manuel Batora, Philip Scharfer, and Wilhelm Schabel*

Multilayer coatings and drying of polymer films are widely used to produce different applications like organic electronics or barrier foils. If the product quality requires separated layers, partial or immiscible systems can be used to avoid interdiffusion between the layers. For the prediction of a possible phase separation of a ternary polymer–polymer–solvent system, it is required to measure or obtain from a data bank the three binary interaction parameters of the system to describe its thermodynamic behavior. This poses a challenge due to the scarce data and measurement techniques for polymer–solvent interaction parameters, but even more for polymer–polymer interaction parameters. In this work, a numerical routine is developed to predict the phase separation for given interaction parameters and is validated with literature results. Subsequently, different ternary polystyrene–poly(methyl methacrylate)–toluene mixtures are prepared and the resulting composition of the phase (or phases) is measured via Raman spectroscopy. The determined equilibrium data are used to fit the binary interaction parameters, which can be used afterward as input parameters for the numerical routine in order to predict the ternary phase diagram of the system.

1. Introduction

The interaction behavior between different functional layers is decisive for the product quality of many multilayer coatings. For some applications, it is crucial for the device function to realize a separated multilayer architecture as it is the case for varnishes or organic electronics. Varnishes consist of several layers with specific functions to inhibit corrosion, control oxygen, and water permeability or to provide aesthetics with color pigments.[1,2] For organic electronic devices, like organic light-emitting diodes, a layer intermixing can even result in a complete device failure due to the negative influence on the charge transport.[3] However, medical applications as well as packaging foils require a mixture of different polymers in order to obtain improved barrier and mechanical properties.[2] Regulating the interdiffusion of polymers enables to control the layer architecture and thus the product quality. A common fabrication method, besides extrusion of the different polymer layers, is wet-film processing due to: low fabrication costs, low material loss, and easy scale-up.[4,5] These fabrication techniques result at least in an architecture of one bottom dry layer (polymer 1) and a wet top film (polymer 2–solvent), meaning that knowledge is required to describe the interdiffusion behavior in ternary polymer–polymer–solvent systems. Therefore, the thermodynamic behavior of the system must be considered first, as previous work has shown that ternary polymer–polymer–solvent systems do not intermix if the two polymers are immiscible—even if both polymers are miscible in the used solvent.[6] This was displayed for a double layer consisting of a dry polystyrene (PS) layer and a wet film of poly(methyl methacrylate) (PMMA) and toluene. While the solvent was distributed over the complete double-layer, even after 93 h no polymer interdiffusion has taken place.[6] On the contrary, the completely miscible polyvinyl acetate-PMMA-toluene system shows a completely different behavior, resulting in an interdiffusion of all components.

In this work, the focus is on the experimental and theoretical investigation of the miscibility behavior of ternary polymer–polymer–solvent systems. The Flory–Huggins lattice model has been widely used in literature to describe thermodynamics of polymer solutions and shall be also applied in this study.[7–10] Besides the molar volumes of the components, the Flory-Huggins model requires a binary interaction parameter to calculate the Gibbs free energy. Since the miscibility behavior of two phases is decisively influenced by this interaction parameter, the influence of different parameters on the interaction parameter is discussed hereafter. One experimental method for the determination of polymer–solvent interaction parameters are gravimetrical sorption–desorption

V.-A. Gracia-Medrano-Bravo, L. Merklein, N. Oberle, M. Batora, Dr. P. Scharfer, Prof. W. Schabel
Institute of Thermal Process Engineering
Thin Film Technology
Karlsruhe Institute of Technology (KIT)
Kaiserstrasse 12, Karlsruhe 76131, Germany
E-mail: victor.bravo@kit.edu; lisa.merklein@kit.edu

The ORCID identification number(s) for the author(s) of this article can be found under https://doi.org/10.1002/admt.202000149.

DOI: 10.1002/admt.202000149

experiments. While a certain activity of the solvent a_S is adjusted in the gas phase, the sorbed solvent volume fraction ϕ_S in the polymer film is measured. The binary Flory–Huggins interaction parameter $\chi_{S,P}$ is fitted by minimizing the squared difference between the measured concentration and the calculated, according to Equation (1).[11–13] Parameter r in Equation (1) represents the relative molecular size of polymer and solvent, meaning the molecular size or the molecular weight has an influence as well as the concentration of the components. It is known that χ a function of the molecular weight is, the exact form of the function is still under discussion. Many authors report for polymer blends, a decreased interaction parameter for an increase of the molecular weight.[14,15] However, Chen et al. observed different molecular mass dependencies for both polymers and explained the contrary trend by the polar/nonpolar character of the used polymer blend.[16] Lau et al. reported for PS-PMMA-Toluene systems, that the increase of the molecular weight results in a reduced polymer–polymer interaction parameter $\chi_{P1,P2}$ and an increase of immiscibility.[17] However, if the molecular weight remains constant, a smaller $\chi_{P1,P2}$ results in a higher miscibility[10,18]

$$\ln a_S = \ln \phi_S + \left(1 - \frac{1}{r}\right) \cdot \phi_P + \chi_{S,P} \cdot \phi_P^2 \tag{1}$$

Furthermore, the $\chi_{S,P}$s have also a minor temperature dependence, due to the enthalpic and entropic contributions to the Gibbs energy.[19] This applies also to the polymer–polymer interaction parameter $\chi_{P1,P2}$, whereby its temperature dependence can be modeled according to Equation (2), using an entropic χ_S and enthalpic χ_H contribution.[20,21] Depending on the material system, χ_H can be either positive or negative, resulting in an increase or decrease, respectively, on the miscibility at higher temperatures. If the $\chi_H > 0$, then $\chi_{P1,P2}$ decreases as the temperature rises. Therefore, the immiscibility region lies under the critical solution temperature T_c (UCST). Thus, at higher temperatures ($T > T_C$) the mixture will be one phase. If the $\chi_H < 0$, then $\chi_{P1,P2}$ increases with the temperature, and the immiscibility region lies above the lower critical solution temperature (LCST).[22–24] From the work of Callaghan and Paul, it is known that PS-PMMA is a UCST system, thus a lower polymer–polymer interaction parameter is expected for increased temperature[25]

$$\chi_{P1,P2} = \chi_S + \frac{\chi_H}{T} \tag{2}$$

For polymer–solvent interaction parameters $\chi_{S,P}$, the increase of temperature increases the entropy allowing more interaction between the molecules and therefore boosting the miscibility.[24]

The measurement of polymer–polymer interaction parameters proves to be a challenge, caused by the aggregate state of the polymers at normal conditions. In literature polymer–polymer interaction parameters are mostly reported for polymer blends (polymers are not dissolved), determined via differential scanning calorimetry or small-angle neutron scattering (SANS).[26,27] The available data make it difficult for accurately predicting phase separation in a ternary polymer solution.

Turbidity measurements using light scattering are typical investigation methods to verify the concentration of the separated phase.[28] Raman spectroscopy is also an interesting characterization tool, as it combines the advantages to measure in situ the local concentration of all components. This measurement technique has already been successfully used by Thien et al. for the determination of liquid–liquid equilibria of multisolvent systems.[29]

In literature, there are often data available for the binary polymer–solvent interaction parameter, but only limited data for the polymer–polymer interaction parameter. In this study, for the first time Raman spectroscopy is used to determine liquid–liquid equilibrium data for polymer–polymer–solvent systems. Both, the influence of polymer chain length and temperature on the miscibility limit is investigated for the PS-PMMA-Toluene system. The polymer–solvent as well as the polymer–polymer interaction parameter have been fitted to the own experimental liquid–liquid (LL) equilibrium data. In addition, a numerical routine is developed that allows the description of ternary phase diagrams for given interaction parameters with no limitations to specific concentration ranges. After the successful validation with the Hsu and Prausnitz[10] phase diagram calculations of model systems, the routine is applied to describe the ternary phase diagram of PS-PMMA-Toluene using the fitted interaction parameters.

2. Theory

First, it is explained how the experimentally determined composition of the two phases is used to calculate the three binary interaction parameters of the system. Subsequently, the numerical routine is presented, which was developed to describe the binodal of the ternary system using the interaction parameters.

2.1. Calculation of Ternary Phase Equilibria

The condition for thermodynamic equilibrium between liquid–liquid phases requires them to have the same chemical potential μ_i^I for each component in the two phases. The chemical potential of each component is calculated by the differentiation of the Gibbs energy of mixing (see Equation (3)) with respect to the number of moles of the respective component as shown in Equation (4). Thereby, n_i represents the moles of each component and m_i the molar volume ratio $\tilde{V}_i / \tilde{V}_S$, whereas $\chi_{i,j}$ are the binary interaction parameters

$$\frac{\Delta^M G}{R \cdot T} = n_{P1} \ln \phi_{P1} + n_{P2} \ln \phi_{P2} + n_S \ln \phi_S + \left(\chi_{P1,P2}\phi_{P1}\phi_{P2} + \chi_{P1,S}\phi_{P1}\phi_S + \chi_{P2,S}\phi_{P2}\phi_s\right)\left(m_{P1}n_{P1} + m_{P2}n_{P2} + m_S n_S\right) \tag{3}$$

for i = P1, P2, S, and I = |, ||

$$\frac{\Delta\mu_i^I}{R \cdot T} = \ln \phi_i + \sum_{j \neq i}\left[\left(1 - \frac{m_i}{m_j}\right) \cdot \phi_j^I\right] + m_i\left[\chi_i \cdot \left(\sum_{j \neq i} \phi_j^I\right)^2 + \sum_{j \neq i} \chi_j \left(\phi_j^I\right)^2\right] \tag{4}$$

where

$$\chi_i = \frac{1}{2}\left(\chi_{i,j} + \chi_{i,k} - \chi_{j,k}\right) \tag{5}$$

The calculation after Hsu and Prausnitz[10] uses the equation system (6), composed of three equations for three volume fractions ϕ_i^I in both phases resulting in six unknown variables, assuming the $\chi_{i,j}$ and m_i are known. The number of unknown volume fractions can be reduced to three, using the solvent concentration as an input variable and the condition of volume fraction, in which the sum of all components in both phases must be one. The resulting three equations are solved to determine the binodal. However, an introduced penalty function excludes the trivial solution, which means that the critical point of the binodal or completely miscible systems cannot be depicted, if the concentrations of both phases reach identical values

$$\Delta\mu_i^{|}\left(\phi_{P1}^{|}, \phi_{P2}^{|}, \phi_S^{|}\right) = \Delta\mu_i^{\|}\left(\phi_{P1}^{\|}, \phi_{P2}^{\|}, \phi_S^{\|}\right) \tag{6}$$

The binary interaction parameters $\chi_{i,j}$ are determined from experimental LL equilibrium data using an objective function with estimated initial values for the interaction parameters. The objective function is built to calculate the squared error between the measured $\phi_{i,\mathrm{exp}}^I$ and calculated $\phi_{i,\mathrm{calc}}^I$ concentration of the respective component according to Equation (7) and is iteratively minimized. This method averages the resulting binary interaction parameters along the composition of the sample. It must be pointed out that, the concentration dependency of $\chi_{i,j}$ is not investigated in the present work, the utilized polymer volume fractions $\phi_{i,\mathrm{exp}}^I$ lie above the overlapping concentration (more information regarding the investigated concentration regime can be found in the Supporting Information).[30–32] Therefore, it can be assumed, that the $\phi_{i,\mathrm{exp}}^I$s in the objective function are in the same concentration regime

$$\mathrm{OBJ} = \sum_I \sum_i \left(\phi_{i,\mathrm{exp}}^I - \phi_{i,\mathrm{calc}}^I\right)^2 \tag{7}$$

2.2. Numerical Method of the Calculation of the Binodal

Due to the limitations of the Hsu and Prausnitz approach, an alternative numerical method was developed to calculate the binodal. This method utilizes the two minima in the Gibbs energy curve for systems with miscibility gap and builds a tangent line in their neighborhood. The calculations for the binodal curve are done by constructing a tangent line to the Gibbs energy curve as a function of the parametrized concentration. The proof of the parametrization of the Gibbs energy can be found in the Supporting Information.

The numerical method consists in discretizing the ternary diagram and checking every single point if it is inside or outside the binodal curve, instead of solving numerically the equation system (6). This method requires no start value and it is not iterative. The criterion for a nonparametrized point to lay inside the binodal curve—thus to be immiscible—is defined as it follows

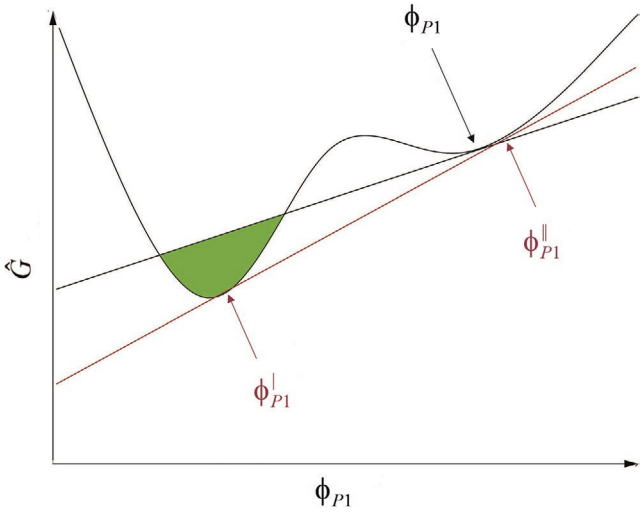

Figure 1. Graphical representation of the tangent criterion for the calculation of the binodal. The tangent line at ϕ_{P1} lies above the Gibbs energy curve of the system, meaning ϕ_{P1} is located within the binodal.

$$\forall\ \phi_S > 0\ \exists\left(\phi'_{\mathrm{P1}} \in [0;1], \phi'_{\mathrm{P2}} \in \left[0;1-\phi'_{\mathrm{P1}}\right]\right):$$
$$\hat{G}(\phi_{\mathrm{P1}}, \phi_{\mathrm{P2}}) + \frac{\partial G}{\partial \phi_{\mathrm{P1}}}\left(\phi'_{\mathrm{P1}} - \phi_{\mathrm{P1}}\right) + \frac{\partial G}{\partial \phi_{\mathrm{P2}}}\left(\phi'_{\mathrm{P2}} - \phi_{\mathrm{P2}}\right) > \hat{G}\left(\phi'_{\mathrm{P1}}, \phi'_{\mathrm{P2}}\right) \tag{8}$$

The 2D volume fraction space is discretized in a lattice. For each lattice point $(\phi_{\mathrm{P1}}, \phi_{\mathrm{P2}})$, values of the tangential plane, defined as the left side of Equation (8), are calculated for each other lattice point $(\phi'_{\mathrm{P1}}, \phi'_{\mathrm{P2}})$ and compared to $\hat{G}(\phi'_{\mathrm{P1}}, \phi'_{\mathrm{P2}})$. If there is any $(\phi'_{\mathrm{P1}}, \phi'_{\mathrm{P2}})$, at which the value of the tangential plane for $(\phi_{\mathrm{P1}}, \phi_{\mathrm{P2}})$ is higher than $\hat{G}(\phi'_{\mathrm{P1}}, \phi'_{\mathrm{P2}})$, then $(\phi_{\mathrm{P1}}, \phi_{\mathrm{P2}})$ is considered inside the binodal, otherwise outside.

In **Figure 1**, a slice of $\hat{G}$ function is shown in a 1D space, similar as it were parametrized. Following the criterion, a tangential line at a point ϕ_{P1} would lay over the Gibbs energy curve (shown in green) and therefore inside the binodal. Consequently, phase separation occurs causing two coexisting phases with the polymer volume fractions $\phi_{\mathrm{P1}}^{|}$ and $\phi_{\mathrm{P1}}^{\|}$. The binodal curve is built by marking the transition points, where the criterion is not fulfilled, as a boundary. The numerical method was programed in a 2018b MATLAB routine with the molar volume ratios m_i and the binary interaction parameters $\chi_{i,j}$ as input values. The method has a computing time of 5 min for a discretization with 400 points for $(\phi_{\mathrm{P1}}, \phi_{\mathrm{P2}})$, resulting in 80 000 concentration points. The solvent concentration is calculated by solving the volume fraction from the unity sum condition, negative values for ϕ_S are not considered for the discretization and are substituted with zeros. As the approach to construct tangents lines, proves if the respective point in the ternary phase diagram is located inside or outside of the binodal, the method does not consider the possibility of a three-phase coexistence until now.

3. Experimental Investigation of Liquid–Liquid Equilibria in Polymer–Polymer–Solvent Systems

3.1. Inverse Raman Spectroscopy Measurements

The investigated ternary samples are prepared and treated as mentioned in the Experimental Section. The prepared concentrations as well as molar masses of the used polymers are given in Table 2. The samples are prepared in transparent glass vials and their Raman intensity is measured with a special setup described in **Figure 2**. The attachment has a screw at the bottom, which allows measuring the intensity at different heights in the vial. The phase boundary can be detected optically using the internal camera of the microscope and was set as reference for the concentration measurements of the two phases. The supplementary Raman-measurements are performed at three different vertical positions in both phases in order to evaluate, if the phases are homogenous. The concentration of each component is determined by superposing the intensity of the spectra of the pure components I_i in a weighted sum,[33] as shown in Equation (9). The weighting factors ω_i are calculated by minimizing the sum of squared differences between measured and calculated spectrum

$$I_{\text{mixture}} = \omega_{\text{PS}} \cdot I_{\text{PS}} + \omega_{\text{PMMA}} \cdot I_{\text{PMMA}} + \omega_{\text{Tol}} \cdot I_{\text{Tol}} \tag{9}$$

where

$$\omega_{\text{PS}} + \omega_{\text{PMMA}} + \omega_{\text{Tol}} = 1 \tag{10}$$

The Raman intensity is converted to a concentration value by measuring the Raman spectra of calibration samples with a known polymer loading $X_{i,\text{Tol}}$ and fitting the calibration constant $K_{\text{i,Tol}}$ using Equation (11).[33] The pure component spectra and the calibration curves are provided in the Supporting Information

$$\frac{\omega_i}{\omega_{\text{Tol}}} = K_{\text{i,Tol}} \cdot X_{i,\text{Tol}} \tag{11}$$

For i = PS, PMMA

In Figure 2 (right), an exemplary concentration measurement is shown for a prepared sample with 76.4 v% toluene. While a PMMA concentration of 27.9 ± 0.5 v% could be measured in the bottom phase, a PS concentration of 20.7 ± 0.4 v% could be determined in the upper phase. The system has separated almost into two binary phases, in both cases only a negligible concentration of less than 0.5 v% of the other polymer can be detected. At the phase boundary, a change in the solvent concentration of 5 v% can be observed due to the different LL equilibria. More information regarding the measurement technique can be found in Scharfer, Schabel et al.[34–36]

4. Results and Discussion

First, the developed calculation routine is validated via the results from Hsu and Prausnitz[10] for a fictitious polymer–polymer–solvent system. Subsequently, the coexisting phase compositions measured via Raman spectroscopy are shown and used to calculate the three binary interaction parameters $\chi_{i,j}$, enabling plotting of the binodal of the PS-PMMA-Toluene system. Furthermore, the influence of a higher temperature and a lower molar mass of both polymers is investigated on the miscibility of the system.

4.1. Validation of the Numerical Method

The developed numerical method (described in Section 2.2) was compared with the method described by Hsu and Prausnitz[10] to determine its accuracy. In **Figure 3** (solid lines), the binodals of four ternary systems are plotted using the same molar volume ratio and polymer–polymer as well as polymer 1-solvent interaction parameters, while the polymer 2-solvent parameter is increased from (a) to (d). This investigation of Hsu and Prausnitz shows the increase of immiscibility for increasing polymer–solvent interaction parameter, if the molar volume ratios stays constant. In Figure 3 are also the binodals displayed, which are calculated with the developed MATLAB

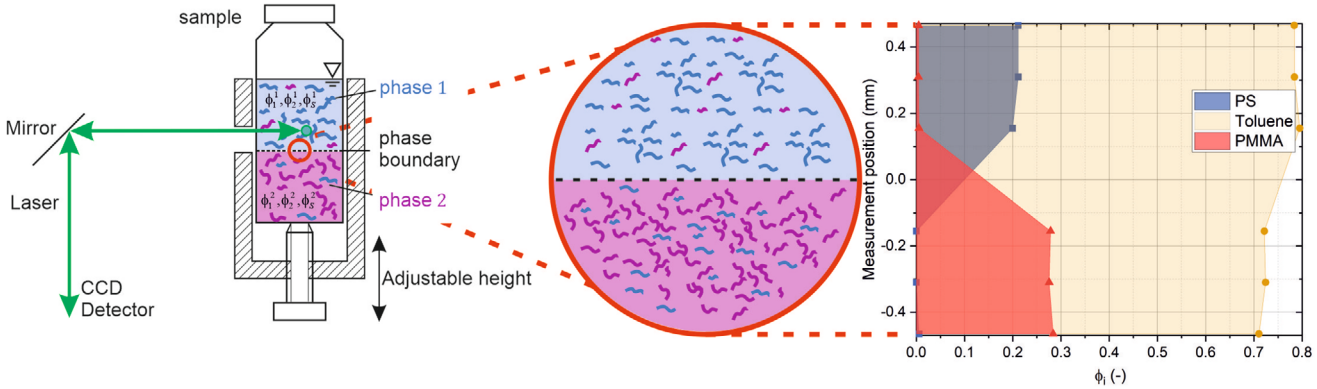

Figure 2. Experimental set-up for the concentration measurements. Three Raman measurements were performed in both phases to evaluate the homogeneity, whereby the phase boundary could be detected optically (see Figure 6). On the right side, an exemplary concentration profile is shown for all three components.

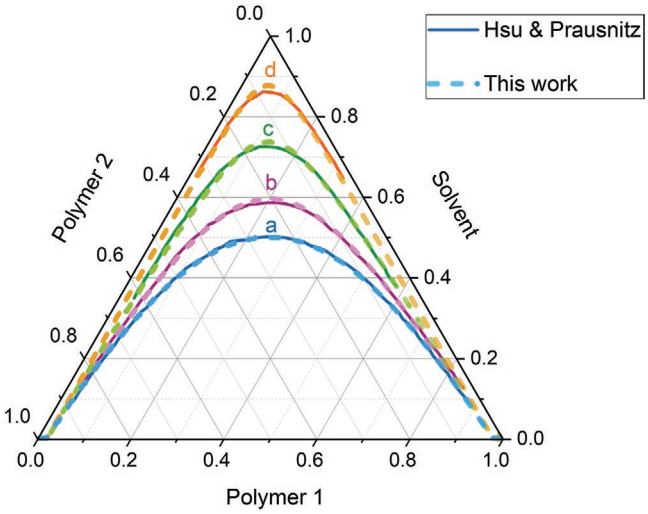

Figure 3. Comparison between the miscibility limits calculated by Hsu and Prausnitz[10] (solid lines) and in this work (dashed lines) for the same model system. The used model system parameters are $m_1 = m_2 = 1000$, $\chi_{1,2} = 0004$; $\chi_{1,S} = 0{,}4$; $\chi_{2,S} =$ a) 0,4; b) 0,44; c) 0,46; d) 0,48. Adapted with permission.[10] Copyright 1974, American Chemical Society.

routine (dashed lines), using the same input parameters as Hsu and Prausnitz. A comparison proves a good agreement between both simulation approaches, thus a successful validation of the developed routine.

4.2. Calculation of Ternary Phase Diagrams Using the Measured LL Equilibrium Data

In literature, PS-PMMA-Toluene is known to be immiscible up to a toluene content of 80 v% or more, depending on the molar masses of the polymers.[37] For this reason, the measurements regarding the investigation of the miscibility limit of this system were done at high solvent concentrations. On the left side of **Figure 4**, the measured concentrations of the coexisting phases are plotted in a ternary phase diagram as white-filled symbols, whereas the prepared concentration is marked in purple. The slight discrepancy from the intended concentration and the position of the conode can be explained due to solvent evaporation and the deviation from the calibration constant $K_{i,\mathrm{Tol}}$. The LL-equilibrium data are used to fit the three binary interaction parameters with Equation (7), the resulting values are given in **Table 1** (L20). On the right side in addition to the experimental LL-equilibrium data, the binodal calculated with the mentioned interaction parameters is shown in green. Most of the measured phase concentrations lay on the calculated curve at low solvent concentrations and with less than 3 v% deviation at high solvent concentrations. No phase separation is visible for the blend with the highest investigated solvent content (95 v%). All the measurements are used to calculate the binary interaction parameters $\chi_{i,j}$. Each liquid phase was measured three times at different positions to ensure there were no concentration gradients. The error bars are not visible in Figure 4, due to the resolution of the image. The calculated binodal is determined using the numerical method described in Section 2.2.

The influence of temperature and polymer chain length was also investigated to show the flexibility of both, the numerical method and the experimental determination of $\chi_{i,j}$. In **Figure 5**, the results are plotted in ternary diagrams. On the left side, the PS192k-PMMA120k-Toluene system was measured at 20 °C (L20) and 40 °C (L40) in order to investigate the temperature influence on the miscibility behavior. As discussed in the Introduction, an increased miscibility is expected for a higher temperature. The results confirm this hypothesis: the long chain system at 40 °C (red curve) shows a slight increase of the miscibility at lower solvent content compared to the miscibility gap at 20 °C (green curve), due to an entropy increase at higher temperatures. On the right side, the experimental LL-equilibrium data as well as the calculated binodals of the long polymer chain system (PS192k-PMMA120k-Toluene) in green (L20) and a short polymer chain system (PS35k-PMMA15k-Toluene) in yellow (S20) are shown in order to discuss the influence of the molar mass at 20 °C. The increase of miscibility at a smaller chain size is considerable, as a result of the decrease

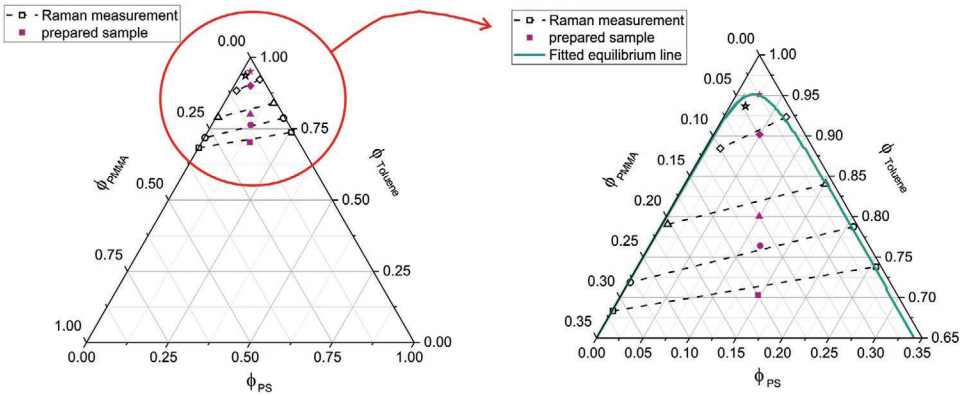

Figure 4. Ternary phase diagram of the PS192k-PMMA120k-Toluene system at 20 °C. Left: The prepared samples are shown in purple, while the measured average concentrations are displayed in black. The dashed lines indicate the two related phases. The same symbol characterizes, which separated phases belong to which sample. Right: Zoom of the left diagram including equilibrium line which is fitted to the measured concentration of the separated phases.

Table 1. Binary interaction parameters fitted using the Raman LLE-data for ternary PS-PMMA-Toluene systems by varied temperature and molar mass. In the last row, a literature value range is given for every binary interaction parameter of this system.[17,27,32,38–40]

Sample	Temperature [°C]	Molar mass [kg mol^{-1}]		$\chi_{PS,PMMA}$	$\chi_{PS,Tol}$	$\chi_{PMMA,Tol}$
		PS	PMMA			
L20	20	192	120	3.70×10^{-3}	0.541	0.581
L40	40	192	120	3.26×10^{-3}	0.378	0.476
S20	20	35	15	1.62×10^{-2}	0.275	0.444
[38]	124	96.2			0.322	
[32]	28	244			0.430	
[32]	28		129			0.450
[27]	25	24.5	39.3	1.7×10^{-2}		
[17]	23	100	180	$6.8–23.5 \times 10^{-3}$	0.398–0.409	0.448
Literature range	23–150	9–190	18–211	$6.8–29 \times 10^{-3}$	0.322–0.868	0.448–0.947

of polymer repulsion interactions at low molecular mass. While the miscibility gap starts at a solvent concentration of 95 v% for the long chain system, the miscibility gap decreases to a solvent content of 65 v% due to the shorter polymer chains. Unfortunately, for low chain size, the numerical method did not predict the S20 system as well as for the other cases. It is assumed that for S20 the interaction parameters have to be considered concentration-dependent. The fitted binary interaction parameters for L40 as well as S20 are given in Table 1.

As known in literature (see Table 1), the fitted PS-PMMA interaction parameters are 1–2 orders of magnitude below the determined polymer–solvent interaction parameters. The influence of temperature and molar mass on the miscibility gap can also be discussed by comparing the fitted interaction parameters. As expected for a UCST system, there is a small decrease for the binary polymer–polymer interaction parameters if the temperature is increased from 20 to 40 °C. In addition, both polymer–solvent interaction parameters decrease for the raised temperature, indicating an enhanced miscibility at 40 °C compared to the miscibility behavior at 20 °C.

The reduction of the molar mass (S20) leads to smaller polymer–solvent interaction parameters compared to the values of L20, but to a remarkable increase of the PS-PMMA interaction parameter—five times—compared to L20. The effect of an increased polymer–polymer interaction parameter for lower molar masses follows the same trend reported by Lau et al.[17] This trend is explained by the increased number of contacts points caused by the increment in the polymer mobility. It can be stated that all interaction parameters determined based on the own LL equilibrium data are within the literature range, which is given in Table 1. The different values for the binary interaction parameters of the same material system can be explained by the influence of concentration, molar mass, and temperature as well as the used measurement technique. The literature data[27,32,38–40] given in Table 1 for polymer–solvent systems were determined using sorption measurements, gas chromatography, or intrinsic viscosity considerations, while differential scanning calorimetry has been used for the investigation of the polymer blends. Furthermore, investigations are performed via gel permeation chromatography regarding the ternary PS-PMMA-Toluene system.[17]

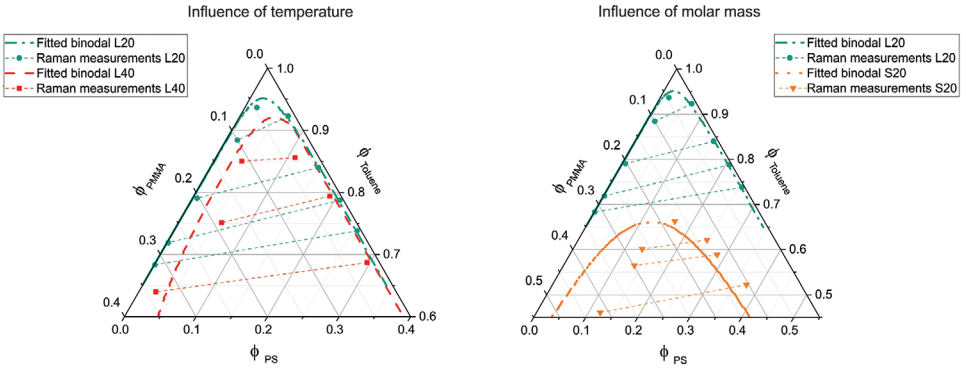

Figure 5. Temperature and polymer chain size comparison. Left: Ternary phase diagrams for the PS192k-PMMA120k-Toluene system at 20 °C plotted in green (L20) and 40 °C in red (L40), showing a small increase of the miscibility. Right: Ternary phase diagrams at 20 °C for the PS192k-PMMA120k-Toluene system in green (L20) and PS35k-PMMA15k-Toluene system in yellow (S20) showing a considerable increase of the miscibility for shorter polymer chains.

5. Conclusion

In the present work, Raman spectroscopy was utilized to measure the concentration of the single components in the ternary system PS-PMMA-Toluene at different solvent contents to determine LL equilibrium data, if the blends separate into two coexisting phases. The three binary interaction parameters of the system were fitted to the experimental LL equilibrium data via the least square method. Furthermore, a new numerical method was developed to calculate the binodal of ternary polymer–polymer–solvent systems, using only the molar volume ratios and binary interaction parameters of the systems. After the validation with the approach made by Hsu and Prausnitz, we used the own determined interaction parameters in order to describe the ternary phase diagram of PS-PMMA-Toluene. The system was investigated at a higher temperature as well as with shorter polymer chains in order to show the influence of these parameters on the miscibility. In particular, the decrease of the chain lengths from PS192k-PMMA120k to PS35k-PMMA15k leads to an increase of the miscibility, thus the critical point is decreased from a solvent content of 95 to 65 v%. As the interaction parameters determined based on the own LL equilibrium data are within the literature range for comparable polymer chain sizes, it can be concluded that noninvasive Raman spectroscopy gives a new alternative for the experimental determination of binary interaction parameters $\chi_{i,j}$. The advantage of our procedure is time saving as only a few measurements are necessary to fit the three binary interaction parameters of the system. In future work, the concentration dependency will be addressed to predict the phase separation of ternary systems.

6. Experimental Section

Chemicals and Materials: Toluene was purchased from Merck KGaA (Darmstadt, Germany, SeccoSolv, 99,9%). Poly(methyl methacrylate) PMMA (M_w 15 000; 120 000 g mol^{-1}) and Polystyrene PS (35 000; 192 000 g mol^{-1}) were used as received from Sigma-Aldrich (Munich, Germany).

Sample Preparation: Ternary PS-PMMA-Toluene mixtures were prepared in glass vials (2 mL) from WICOM (Heppenheim, Germany) and stirred for 2 weeks in order to dissolve the polymers. All samples were sonicated to remove absorbed air (Emmi-H60, EMAG AG, Mörfelden-Walldorf). Subsequently, the vials were centrifuged using a SIGMA 2-16KC centrifuge (Sigma Laborzentrifugen GmbH, Osterode am Harz) to accelerate the phase separation. The adjusted parameters were 5000 min^{-1} for 12 h at the desired temperature (20 and 40 °C). In **Figure 6**, the samples are shown before centrifugation on the left side and after centrifugation on the right side.

The prepared and investigated ternary concentrations as well as the molar masses of the used polymers are shown in **Table 2**.

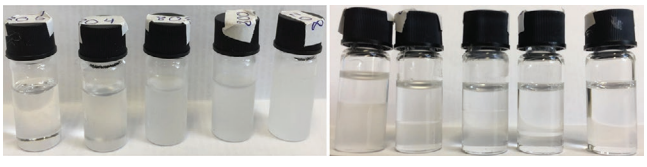

Figure 6. Ternary samples with long polymer chains before (left) and after centrifuging them (right), where the phase boundary is visible.

Table 2. Composition and polymer molar weights for each sample.

Nr.	$\tilde{M}_{PS}$ [kg mol^{-1}]	$\tilde{M}_{PMMA}$ [kg mol^{-1}]	ϕ_{Tol}	ϕ_{PS}	ϕ_{PMMA}
400	35	15	0.840	0.080	0.080
401	35	15	0.500	0.250	0.250
402	35	15	0.610	0.200	0.200
403	35	15	0.700	0.150	0.150
404	35	15	0.800	0.100	0.100
405	35	15	0.950	0.025	0.025
406	35	15	0.650	0.175	0.175
800	192	120	0.760	0.120	0.120
802	192	120	0.700	0.150	0.150
803	192	120	0.800	0.100	0.100
804	192	120	0.900	0.050	0.050
805	192	120	0.950	0.025	0.025

Supporting Information

Supporting Information is available from the Wiley Online Library or from the author.

Acknowledgements

The authors acknowledge the financial support from the German Research Foundation (Deutsche Forschungsgemeinschaft), the German Academic Exchange Service (DAAD), and the National Council of Science and Technology (CONACYT) for the research grant provided.

Conflict of Interest

The authors declare no conflict of interest.

Keywords

binary interaction parameters, liquid–liquid equilibrium, phase diagram, polymer films, Raman spectroscopy

Received: February 21, 2020
Revised: April 24, 2020
Published online:

[1] P. S. Kumar, R. Rajasekar, S. K. Pal, G. C. Nayak, S. M. R. S. Ismail, in *Multicomponent Polymeric Materials*, Vol. *223* (Eds: J. K. Kim, S. Thomas, P. Saha), Springer, Dordrecht **2016**, pp. 157–229.
[2] D. Langhe, M. Ponting, *Manufacturing and Novel Applications of Multilayer Polymer Films*, Elsevier, Amsterdam **2016**.
[3] L. Merklein, M. Mink, D. Kourkoulos, B. Ulber, S. M. Raupp, K. Meerholz, P. Scharfer, W. Schabel, *Technol. Res.* **2019**, *16*, 1643.
[4] R. R. Søndergaard, M. Hösel, F. C. Krebs, J. Polym, *J. Polym. Sci., Part B: Polym. Phys.* **2013**, *51*, 16.
[5] B. Park, O. E. Kwon, S. H. Yun, H. G. Jeon, Y. H. Huh, *J. Mater. Chem. C* **2014**, *2*, 8614.
[6] S. M. Raupp, D. K. Siebel, P. G. Kitz, P. Scharfer, W. Schabel, *Macromolecules* **2017**, *50*, 6819.
[7] H. Tompa, *Trans. Faraday Soc.* **1949**, *45*, 1142.

[8] H. H. Kausch, M. Tirrell, *Annu. Rev. Mater. Sci.* **1989**, *19*, 341.
[9] F. W. Altena, C. A. Smolders, *Macromolecules* **1982**, *15*, 1491.
[10] C. C. Hsu, J. M. Prausnitz, *Macromolecules* **1974**, *7*, 320.
[11] P. J. Flory, *J. Chem. Phys.* **1941**, *9*, 660.
[12] M. L. Huggins, *J. Chem. Phys.* **1941**, *9*, 440.
[13] P. J. Flory, *Principles of Polymer Chemistry*, Cornell University Press, New York **1953**.
[14] D. C. Morse, J. K. Chung, *J. Chem. Phys.* **2009**, *130*, 224901.
[15] A. J. Nedoma, M. L. Robertson, N. S. Wanakule, N. P. Balsara, *Macromolecules* **2008**, *41*, 5773.
[16] Q. P. Chen, S. Xie, R. Foudazi, T. P. Lodge, J. I. Siepmann, *Macromolecules* **2018**, *51*, 3774.
[17] W. W. Y. Lau, C. M. Burns, R. Y. M. Huang, *Eur. Polym. J.* **1987**, *23*, 37.
[18] H. W. Kammer, *Acta Polym.* **1986**, *37*, 1.
[19] T. P. Russell, R. P. Hjelm, P. Seeger, *Macromolecules* **1990**, *23*, 890.
[20] K. H. Dai, E. J. Kramer, *Polymer* **1994**, *35*, 157.
[21] C. C. Han, B. J. Bauer, J. C. Clark, Y. Muroga, Y. Matsushita, M. Okada, Q. Tran-cong, T. Chang, I. C. Sanchez, *Polymer* **1988**, *29*, 2002.
[22] P. Knychała, K. Timachova, M. Banaszak, N. P. Balsara, *Macromolecules* **2017**, *50*, 3051.
[23] H. B. Eitouni, N. P. Balsara, in*Physical Properties of Polymers Handbook*, Vol. *2* (Ed.: J. E. Mark), Springer, New York **2007**, pp. 339–356.
[24] M. Rubinstein, R. H. Colby, *Polymer Physics*, Vol. *23*, Oxford University Press, New York **2003**, p. 137.
[25] T. A. Callaghan, D. R. Paul, *Macromolecules* **1993**, *26*, 2439.
[26] A. J. Nedoma, M. L. Robertson, N. S. Wanakule, N. P. Balsara, *Ind. Eng. Chem. Res.* **2008**, *47*, 3551.
[27] C. M. Burns, W. N. Kim, *Polym. Eng. Sci.* **1988**, *28*, 1362.
[28] L. A. Utracki, C. A. Wilkie, *Polymer Blends Handbook*, Springer, Dordrecht **2014**.
[29] J. Thien, C. Peters, T. Brands, H.-J. Koß, A. Bardow, *Ind. Eng. Chem. Res.* **2017**, *56*, 13905.
[30] J. Rauch, W. Köhler, *J. Chem. Phys.* **2003**, *119*, 11977.
[31] H. Zettl, U. Zettl, G. Krausch, J. Enderlein, M. Ballauff, *Phys. Rev. E* **2007**, *75*, 061804.
[32] C. M. Kok, A. Rudin, *J. Appl. Polym. Sci.* **1982**, *27*, 353.
[33] W. Schabel, *Chem. Ing. Tech.* **2005**, *77*, 1915.
[34] W. Schabel, I. Ludwig, M. Kind, *Drying Technol.* **2004**, *22*, 285.
[35] P. Scharfer, W. Schabel, M. Kind, *J. Membr. Sci.* **2007**, *303*, 37.
[36] D. Siebel, P. Scharfer, W. Schabel, *Macromolecules* **2015**, *48*, 8608.
[37] G. Venugopal, S. Krause, *Macromolecules* **1992**, *25*, 4626.
[38] F. H. Covitz, J. W. King, *J. Polym. Sci. Part A-1: Polym. Chem.* **1972**, *10*, 689.
[39] Y. S. Lipatov, A. E. Nesterov, *Macromolecules* **1975**, *8*, 889.
[40] P. J. T. Tait, A. M. Abushihada, *Macromolecules* **1978**, *11*, 918.